Theoretical Phase Diagrams of Polymer/Clay Composites: The Role of Grafted Organic Modifiers

Valeriy V. Ginzburg, Chandralekha Singh, and Anna C. Balazs*

Department of Chemical and Petroleum Engineering, University of Pittsburgh, Pittsburgh Pennsylvania 15261

Received August 9, 1999; Revised Manuscript Received November 3, 1999

ABSTRACT: We combine a density functional theory (DFT) with a self-consistent field model (SCF) to calculate the phase behavior of thin, oblate colloidal particles that are coated with surfactants and dispersed in a polymer melt. These coated particles represent organically modified clay sheets. By integrating the two methods, we can investigate the effect of the surfactants' characteristics (grafting density ρ_{gr} and length N_{gr}) and the polymer−surfactant interaction energy on the polymer−clay phase diagram. Depending on the values of these critical parameters and the clay volume fraction, ϕ, the system can be in an isotropic or nematic phase (which corresponds to an exfoliated composite). The system can also form a smectic, crystal, columnar, or "house-of-cards" plastic solid, as well as a two-phase (immiscible) mixture. Using this model, we isolate conditions that lead to the stabilization of the homogeneous, exfoliated phases (the isotropic and nematic regions) and to the narrowing of the immiscible two-phase regions.

I. Introduction

The recent interest in polymer−clay nanocomposites stems from the dramatic improvement in physical properties that can be produced by adding just a small fraction of clay to a polymer matrix.[1−13] For example, the addition of 2−5 wt % of clay fillers doubles the tensile strength and the modulus,[4] triples the heat distortion temperature,[4] and reduces the gas permeability by a factor of 2.[3] Since the weight fraction of the inorganic additive is typically below 10%, the materials are also lighter than most conventional composites. The optimal performance of such composites is achieved when the clay fillers are uniformly dispersed in the polymer matrix. Fabricating such homogeneous mixtures, however, poses considerable synthetic challenges. The major difficulty arises from the inherent structure of the clay particles, which are composed of broad, closely stacked silicate sheets. The diameter of the sheets lies typically between 20 and 200 nm, depending on the specific type of clay, and each sheet is roughly 1 nm in thickness. The spacing (or "gallery") between the sheets is also on the order of 1 nm, which is smaller than the radius of gyration of typical polymers. Consequently, there is a large entropic barrier that inhibits the polymer from penetrating this gap and intermixing with the clay. Even when the sheets are successfully separated and interspersed into the polymer matrix, these high-aspect ratio platelets can form ordered or crystalline structures within the polymers or can phase separate from the matrix material. Hence, to create composites with the optimal properties, it is important to determine equilibrium phase diagrams, which reveal how the composition of the mixture effects the thermodynamic stability and morphology of the material.

The issue of describing the phase behavior of polymer−clay mixtures can be divided into two parts: determining the polymer-mediated interactions between the clay sheets, and calculating the phase diagram once these interactions are known. In effect, the problem involves analyzing the system on two different length scales. To obtain information on the nanoscale interactions between the organic modifiers on the clay surfaces and the polymer melt, one can treat the clay sheets as infinite flat surfaces. To probe the macroscale behavior of the entire system, the clay disks are treated as rigid particles dispersed in an incompressible fluid and interacting via excluded-volume and effective long-range potentials. The first problem deals with the properties of polymers confined between the clay surfaces, while the second problem concerns the thermodynamics of anisotropic colloidal particles in a melt or solution.

The behavior of polymer melts in confined geometries (between two parallel plates) has been studied using different theoretical (self-consistent field, Monte Carlo) and experimental (neutron scattering, X-ray diffraction, FTIR) methods. Recently, Vaia and Giannelis[11] used a lattice model and Balazs et al.[14−17] used both numerical and analytical self-consistent field (SCF) theories to calculate free energy profiles as two surfaces are pulled apart within a bath of molten polymers. These calculations indicate whether the mixture will form an intercalated or exfoliated composite, or a phase-separated system. In an intercalated system, the polymers penetrate the galleries and enhance the separation between the plates by a fixed amount; in an exfoliated composite, the sheets are effectively separated from each other and dispersed within the polymer melt. Calculating the complete phase diagram for the large-scale system, however, requires a detailed balance of all the contributions to the free energy, including the translational and orientational entropy of the clay particles, as well as their excluded volume interactions. To properly account for these factors, one needs to turn to theoretical methods that are used to describe the macroscopic phase behavior of colloidal systems.

The thermodynamics of polymer−colloid mixtures has been the subject of many theoretical, computational, and experimental studies.[18−27] In most of the theoretical and computational investigations, the colloidal particles were assumed to be spherical in shape and the Asakura−Oosawa (AO)[18] model was adopted to describe the polymer−colloid mixture. In the AO model, the polymers

10.1021/ma991324e CCC: $19.00
Published on Web 01/15/2000

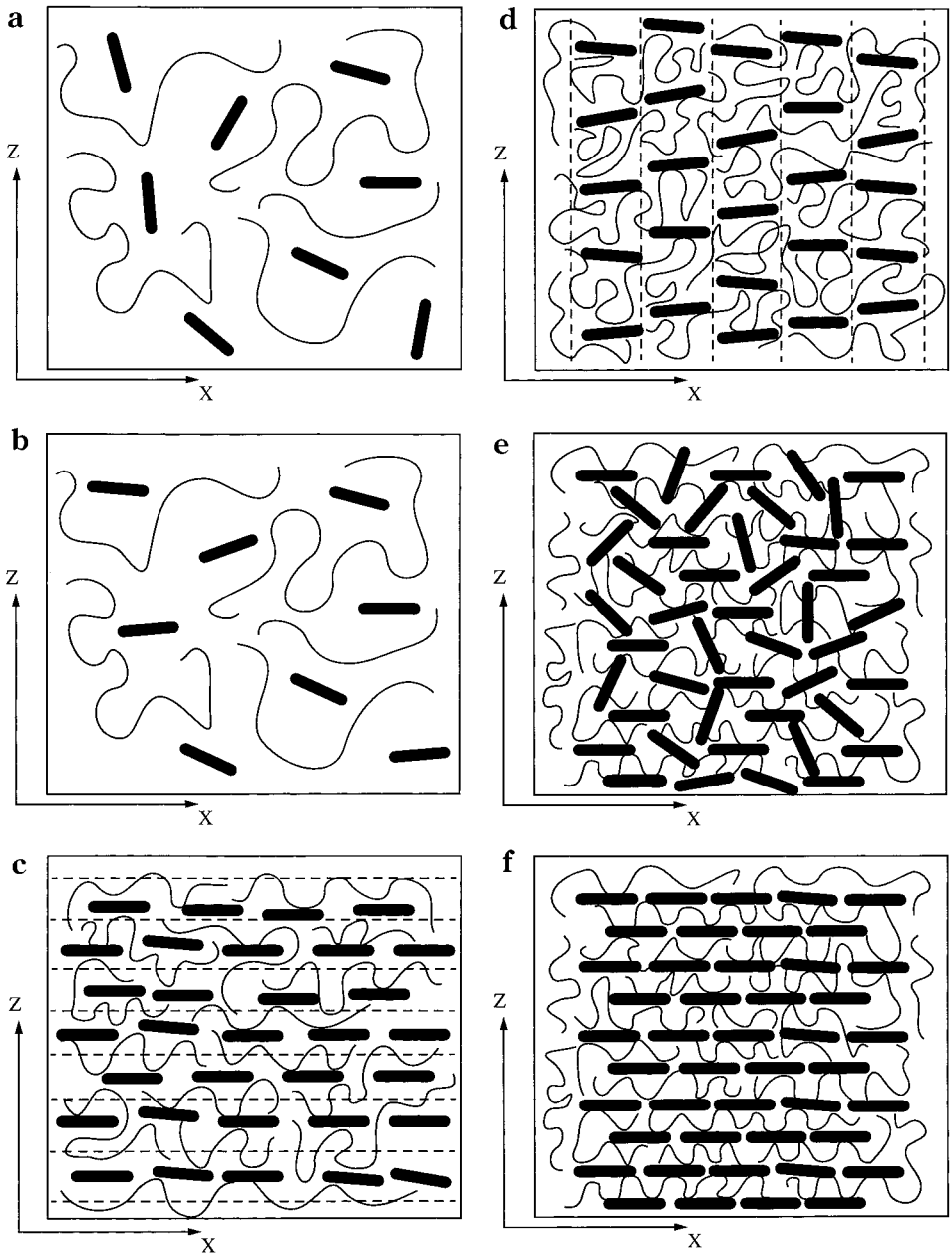

Figure 1. Mesophases of oblate uniaxial particles dispersed in a polymer: (a) isotropic, (b) nematic, (c) smectic A, (d) columnar, (e) plastic solid, and (f) crystal. The nematic director **n** in ordered phases is aligned along the *Z* axis, the disks lie in the *XY* plane. Dashed lines show smectic layers (c) and columns (d).

are represented by small spheres, and the only interaction is due to excluded volume effects. Thus, the problem of characterizing the complex blend was reduced to describing the properties of a binary hard sphere mixture. The phase diagram of binary hard sphere mixtures can be calculated to obtain liquid and solid (colloidal crystal) phases. Calculated phase diagrams can be then tested against experimental data, and good qualitative agreement is generally found between theory and experiment for mixtures of spherical colloids and polymers.[25,27]

In the case of polymer−clay mixtures, however, a complicating factor is introduced by the strong anisotropy in the shape of the clay sheets. As noted above, because of their high aspect ratio, clay sheets experience orientational ordering at low volume fractions and can form liquid crystalline phases (nematic, smectic, columnar, or plastic solid), in addition to traditional liquid and solid phases (see Figure 1). Although there have been a few numerical and experimental studies of the thermodynamics of fluids containing anisotropic colloidal particles,[28−32] the majority of these investigations were focused on rodlike colloids, rather than discotic particles. Dijkstra et al.[31] studied the phase behavior of clay particles (modeled as infinitely thin disks with quadrupolar potentials), and Bates and Luckhurst[32] modeled a system of Gay−Berne[33] disks. Both of these simulations, however, considered only disks in the absence of solvent or polymer.

Recently, Lyatskaya and Balazs[34] and Ginzburg and Balazs[35] developed simple models that describe the liquid crystalline ordering in the polymer−platelet systems. The former theory is based on the Onsager[36] model of the nematic ordering in hard-body fluids, while the latter study uses density functional theory to incorporate the positional (smectic and crystal) ordering of the platelets. By explicitly including excluded volume interactions in these models, one can make direct

correlations between the phase behavior of the system and the geometric properties of the colloidal particles, unlike the more phenomenological Landau-type[37] or Maier−Saupe-type[38,39] theories. In particular, the models of refs 34 and 35 were used to study the role of the clay shape anisotropy and polymer chain length on the overall phase diagram. These theories, however, take into account the long-range interactions between the clay sheets only in a rather approximate manner. An important task that remains is to incorporate a more accurate description of the polymer mediated clay−clay interactions into the density functional approach and, thus, obtain the direct dependence of the phase behavior on chemical and molecular characteristics of the mixture.

In this paper, we combine, for the first time, the density functional formalism for the ordering of the clay sheets with the SCF-calculated potential for the effective clay−clay interactions within a polymer melt. We incorporate this potential into the Somoza−Tarazona[40,41] free energy functional for anisotropic oblate ellipsoids of revolution. The model is used to describe the phase diagram for several systems of clay disks with grafted organic modifiers, or "surfactants", dispersed in a polymer melt. When the polymer−surfactant interaction is attractive, the effective interaction between the clay sheets becomes repulsive, and intercalation can take place. For a repulsive interaction between the polymers and surfactants, the effective clay−clay interaction becomes attractive, and the system is driven toward phase separation between the pure polymer and clay. By varying the clay volume fraction, ϕ, and the strength of the polymer−surfactant interaction, χ, we obtain the phase diagrams for several values of the surfactant grafting density, ρ_{gr}, and length, N_{gr}.[42] The resulting phase diagrams not only confirm the earlier qualitative predictions[14,16] but also offer quantitative estimates of the volume fractions of clay corresponding to different phases.

II. Theory

A. The Model. We consider a system of clay disks with a thickness $L = 1$ nm and diameter $D = 30$ nm (values similar to the experimental system of Muzny et al.[13]) dispersed in a polymer melt where the length of the chains is given by $N = 300$. Short organic modifiers, or surfactants, are grafted to the surface of each clay platelet; the length of the surfactants is given by N_{gr} and surface density of these chains is specified by ρ_{gr}. Both the polymers and the surfactants are taken to be flexible Gaussian chains. Each monomer of either the surfactant or bulk polymer is modeled by a sphere of radius $a = 1$ nm. The polymer−polymer interactions and the surfactant−surfactant interactions are restricted to excluded-volume effects. On the other hand, the interaction between the polymers and surfactants consists of excluded-volume interactions and a short-range enthalpic term modeled by the Flory−Huggins lattice approximation.[43] The Flory−Huggins parameter χ describes the strength of the interaction between the polymer and the grafted surfactant and depends on the temperature and the chemical structure of both materials.

To study the dependence of the phase behavior of the mixture on the volume fraction of clay, ϕ_c, and the Flory−Huggins parameter, χ, we use the Somoza−Tarazona[40,41] formulation of the density functional theory (DFT). This formalism was first developed for monodisperse fluids of rigid anisotropic particles. To adapt it to binary or ternary systems (colloidal particles dispersed in polymer melt or solution), we follow ideas developed in refs 44 and 34 and impose the incompressibility condition

$$\phi_c + \phi_{gr} + \phi_p = 1 \tag{1}$$

for the case of a polymer melt, and

$$\phi_c + \phi_{gr} + \phi_p + \phi_s = 1 \tag{2}$$

for the case of a polymer solution. Here, ϕ_{gr} is the volume fraction of the grafted organic surfactant, ϕ_p is the volume fraction of the polymer, and ϕ_s is the volume fraction of the solvent. In this paper, we consider only the case of the polymer melt, so that $\phi_s = 0$.

The volume fractions of clay and surfactant are related via

$$\phi_{gr} = \frac{\phi_c}{V_c}\rho_{gr}N_{gr} \tag{3}$$

where $V_c = (\pi/6)D^2L$. Here, we consider the clay sheets to be thin, oblate ellipsoids of revolution, rather than oblate cylinders or cut spheres. This approximation allows us to use the Somoza−Tarazona free energy density functional without introducing additional adjustable parameters. (Although our specific choice for the shape of the clay can affect the phase behavior for large volume fractions of clay, the general features of the phase diagram should remain relatively insensitive to differences between these various geometries. We will explore this point further in future studies.)

We can describe the state of the polymer and organically modified clay mixture by only two variables, χ and ϕ_c (in the following, we will drop the subscript and use ϕ instead of ϕ_c). The orientational and positional ordering of the clay sheets is described by the single-particle distribution function (SDF) $\gamma(\mathbf{r},\mathbf{n})$, where $\mathbf{r}$ represents the position of the center of mass of a particle, and $\mathbf{n}$ is the nematic director (which denotes the direction of the short axis of a disk). Following Kventsel et al.,[45] we decouple the orientational and positional degrees of freedom

$$\gamma(\mathbf{r},\mathbf{n}) = \rho(\mathbf{r})f(\mathbf{n}) \tag{4}$$

where $\rho(\mathbf{r})$ is the positional SDF, and $f(\mathbf{n})$ is the orientational SDF. The free energy of the system is written as a functional of ρ and f.

It is important to note that such an approximation (neglecting the compressibility of the mixture and assuming that the free energy depends only on the clay SDF) is a significant simplification. Recent studies of binary hard-sphere mixtures[26] showed that the "one-density" approach is reasonable when the ratio of the volumes of large and small spheres is sufficiently high. In our system, the volume of a colloidal particle is significantly larger than the volume occupied by a polymer chain, thus justifying the use of a "one-density" approach. The free energy contributions due to the translational and conformational degrees of freedom of the polymer are added only as new terms in the entropic and enthalpic parts of the overall free energy. While the calculation of the translational part of the polymer free energy is straightforward (we simply use a Flory−

Huggins expression), the evaluation of the conformational part is more complicated. Indeed, the conformational entropy of a polymer is strongly dependent on the spatial distribution of dispersed clay particles. Polymers confined in a narrow gallery between two adjacent disks have much smaller entropy than those remaining in the melt. The conformational free energy of the confined polymers can be rewritten as an effective interaction between the disks. This effective interaction can be calculated by using, for example, a numerical self-consistent field (SCF) model.[46−48] Other possible methods of calculating the effective interaction can include an analytical SCF theory,[49] the polymer reference interaction site method (PRISM),[50,51] the direct enumeration of surfactant chain conformations,[52] or Monte Carlo simulations. In this paper, we use the numerical SCF approach.

B. Free Energy Density Functional. The density functional approach is based on a theorem that the free energy of a system can be written as a functional of the single-particle distribution function (SDF). In statistical mechanics, it was first developed by Ramakrishnan and Yussouf.[53] For rigid anisotropic particles, such as those considered here, the SDF is a function of both a spatial coordinate **r** and orientation **n**. The free energy is typically written in the form

$$\beta F = \beta F_{id} + \beta F_{ster} + \beta F_{int} \tag{5}$$

where F_{id} is the free energy of an "ideal gas" of colloidal particles and polymers, F_{ster} is the contribution due to the excluded volume effects for the colloidal (clay) sheets, F_{int} represents the long-range (attractive or repulsive) interactions between clay sheets, and $\beta = 1/kT$.

The first ("ideal") term of the free energy in the rhs of eq 5 can be written as the sum of two parts

$$\beta F_{id} = \beta F_c + \beta F_p \tag{6}$$

In specifying the exact form of βF_c and βF_p, we follow the principles used, for example, by Gast et al.,[20] and Lekkerkerker et al.[23] for the mixtures of polymers and spherical colloidal particles. This approach is modified to include orientational ordering of the clay particles. The "ideal" free energy of clay particles, βF_c consists of translational and orientational terms

$$\beta F_c = \int d\mathbf{r}\, [\rho(\mathbf{r}) \ln(\Phi(\mathbf{r})) + \rho(\mathbf{r}) \int d\mathbf{n}\, f(\mathbf{n}) \ln(4\pi f(\mathbf{n}))] \tag{7}$$

where the "effective clay volume fraction" $\Phi(\mathbf{r}) = \phi + \phi_{gr}$. The "ideal" free energy of the polymer melt, βF_p, includes only the translational (Flory−Huggins) contribution

$$\beta F_p = \frac{\nu}{N v_m}(1 - \Phi) \ln(1 - \Phi) \tag{8}$$

where ν is the total volume of the system, v_m is the monomer volume and $1 - \Phi$ is the volume fraction of the polymer.

We introduce a new parameter, the effective particle thickness L_{eff}

$$L_{eff} = L + 2\rho_{gr} N_{gr} \tag{9}$$

and the effective shape anisotropy parameter $\kappa = L_{eff}/D \leq 1$. The minimal volume occupied by an organically modified particle (if the grafted chains were to form a monolayer) is $V_{eff} = \pi/6 D^2 L_{eff}$.

For a system of ellipsoidal particles, a semiempirical steric interaction free energy can be written as[40,41,54,55]

$$\beta F_{ster} = \int d\mathbf{r}\, \rho(\mathbf{r}) \Psi_{hs}(\bar{\Phi}_c(\mathbf{r})) \frac{V_{excl}[f]}{V_{phe}} \tag{10}$$

where $\Psi_{hs}(x)$ is the semiempirical Carnahan−Starling[56] function, which describes the excess (nonideal) free energy density for hard spheres as a function of their packing fraction. The parameter $V_{excl}[f]$ is the average excluded volume per particle for a given orientational distribution, and $V_{phe} = V_{eff}$ is the excluded volume per particle for perfectly aligned ellipsoids. If we consider only spatially uniform phases (e.g., isotropic and nematic phases), eq 10 would reduce to the Onsager-type expression with the correct second virial coefficient. For nonuniform phases, it is a complicated functional of the density, because the function $\Phi(\mathbf{r})$ depends on $\rho(\mathbf{r})$ in a nontrivial manner (for more details see Appendix A and refs 40 and 41). The role of this functional is to properly describe the short-range correlations due to the excluded volume interactions.

The sum of the free energy terms in eqs 6 and 10 describes an athermal dispersion of hard oblate ellipsoids in a polymer melt. It is known that such a system is capable of forming liquid crystalline (nematic) and crystalline phases.[29,57] To obtain additional liquid crystalline phases (smectic or columnar), strongly anisotropic long-range interactions are required.[58] We suppose that the interaction free energy, βF_{int}, is "small" compared to the ideal and steric free energy terms, i.e., $|\beta F_{int}| < |\beta F_{id} + \beta F_{ster}|$. In this case, one can assume that the pair correlation function for the particles, $g(1,2)$, is mostly determined by the excluded volume effects (not long-range interactions), and calculate the interaction free energy βF_{int} as

$$\beta F_{int} = {}^1/_2 \int d\mathbf{r_1}\, d\mathbf{r_2}\, d\mathbf{n_1}\, d\mathbf{n_2}\, \rho(\mathbf{r_1})\rho(\mathbf{r_2}) f(\mathbf{n_1}) f(\mathbf{n_2}) \delta(1 - \mathbf{n_1}\mathbf{n_2}) g(1,2) V(\mathbf{r_1} - \mathbf{r_2}) \tag{11}$$

where the mean-field pair correlation function $g(1,2) = 0$, if particles overlap, and is equal to 1 if they do not overlap. This form is similar to the traditional way of representing enthalpic interactions between anisotropic particles (see, e.g., eq 3 in ref 55). The δ-function in the rhs of eq 11 allows only those configurations in which interacting disks are parallel. Such an approximation is reasonable for very anisotropic particles where side-by-side configurations have a significantly larger "contact" area than either side-to-edge or edge-to-edge configurations. In addition, since this potential is highly anisotropic, it is likely to promote formation of smectic and columnar phases.[58] The potential function $V(\mathbf{r})$ is assumed to have the following generic form

$$V(\mathbf{r}) = (\pi/4) D^2 (1 - [r_\perp/D]^2) U(z) \tag{12}$$

where $\mathbf{r} = (x, y, z)$, and $r_\perp = (x^2 + y^2)^{1/2}$. The form of the interaction potential per unit area, $U(z)$, and its dependence on such factors as the Flory−Huggins parameter, χ, the polymer chain length, N, the grafting density of the surfactant, ρ_{gr}, and the surfactant chain length, N_{gr}, is discussed in the next section.

When evaluating the integral over positions and orientations of particles (the rhs of eq 11), we use the orientational lattice approximation (see, e.g., ref 59). In this approach, particle orientations are restricted to being along the *x*, *y*, or *z* directions only. Such an approximation is necessary to reduce the number of degrees of freedom and thus, make it possible to analyze the whole phase diagram within a reasonable time frame. (The errors introduced by using the orientational lattice cannot significantly alter the phase diagram since they contribute only to βF_{int} and not to the dominant term βF_{ster}; however, it is possible that the use of the orientational lattice approximation slightly affects the equilibrium value of the nematic order parameter in the ordered phases.)

To describe the thermodynamic behavior of the system, it is necessary to minimize the free energy for all possible phases (isotropic, nematic, smectic, columnar, and crystal) for each value of ϕ_c and find the lowest energy state. After that, coexistence regions can be found by means of applying the Maxwell rule, or, equivalently, by equating the chemical potentials of the particles and the polymer for the different phases. The minimization is done using a variational approach in which the SDF is parametrized by specific functions that reflect the symmetry of a given phase. We use the following parametrization.

For orientational SDF:

$$f(\mathbf{n}) = \frac{\alpha}{4\pi \sinh \alpha}\cosh(\alpha \cos(\mathbf{n},\mathbf{z})) \tag{13}$$

For positional SDF:

$$\rho(\mathbf{r}) = \rho A \exp(L \cos(Q_z z)), \quad \text{for the smectic A phase} \tag{14}$$

$$\rho(\mathbf{r}) = \rho A \exp(L \cos(Q_x x) \cos(Q_y y)), \quad \text{for the columnar phase} \tag{15}$$

$$\rho(\mathbf{r}) = \rho A \exp(L \cos(Q_x x) \cos(Q_y y) \cos(Q_z z)), \quad \text{for the crystal phase} \tag{16}$$

In each case, *A* is a normalization constant, while *L* describes the strength of the positional ordering. To minimize the number of free parameters, we assume that the columnar structure is hexagonal ($Q_x = \sqrt{3}Q_y$), and the crystal structure is "stretched" hexagonal close packed ($Q_x = \sqrt{3}Q_y = \kappa\sqrt{3}Q_z$).

C. Self-Consistent Field Method and Pair Interactions. To complete the free energy functional, it is necessary to calculate the interaction potential per unit area, $U(z)$, for the clay sheets. As mentioned above, this interaction potential consists of two parts: (1) the interaction between "bare" clay particles, $U_1(z)$, (due to electrostatic and van der Waals attraction) and (2) the contribution from the polymer chains confined in the gallery between adjacent clay sheets, $U_2(z)$. (Both contributions are schematically shown in Figure 2). The former term depends on the chemical structure of the clay itself, and we will not attempt to calculate it from first principles (such a calculation is described, for example, in ref 60). Instead, we simply assume that it is purely attractive and short-ranged, and use the following form:

$$U_1(z) = E_0\{1 - \exp(-[z - L_{eff}])\} \tag{17}$$

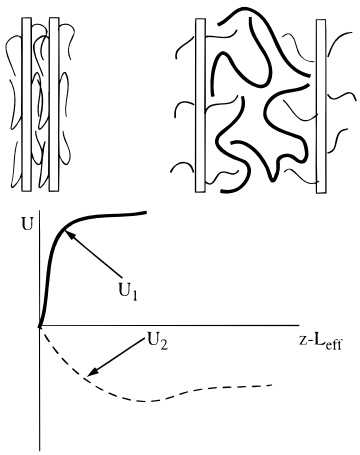

Figure 2. Schematic representation of the pair interaction between the two parallel plates with grafted organic modifiers. The solid line represents the contribution from the "bare plate" attraction, U_1, and the dashed line depicts the effective contribution of the grafted "surfactants" and the polymer chains, U_2. On the sketch, short thin lines are surfactant chains, and long thick lines are "free" chains.

To evaluate the pair interaction between clay sheets due to the presence of the polymers and grafted chains, we employ the self-consistent field method of Scheutjens and Fleer.[46−48] In this method, the phase behavior of polymer systems is modeled by combining Markov chain statistics with a mean-field approximation for the free energy. The equations in this lattice model are solved numerically and self-consistently. Using this model, we consider two infinite parallel plates at a distance *z* apart, immersed in a bath of molten polymer. The short surfactant chains are grafted uniformly on each of the two plates with a grafting density ρ_{gr}. After solving the equations and finding the equilibrium polymer and surfactant density profiles, we calculate the free energy density F/A for each value of the plate separation *z*. Repeating this calculation for different separations, one obtains the effective potential per unit area, $U_2(z)$. The shape of this potential depends on *N*, the polymer chain length, ρ_{gr}, N_{gr}, and the different Flory−Huggins interaction parameters. In this study, we have only one nonzero χ-parameter, that between the polymer and the surfactant. When the interaction between the polymers and surfactants is repulsive (positive χ), the polymers do not penetrate the gallery between the clay sheets, and the effective interaction between the sheets is predominantly attractive. When χ is negative, the interaction between the polymers and surfactants is attractive, and the polymer is pulled into the gallery, leading to the intercalation or possible exfoliation of the clay platelets. The SCF calculation of the interparticle potentials and the qualitative discussion of their influence on the morphology of the polymer/clay composites is discussed in more detail elsewhere.[14−16]

The use of the self-consistent field approach to calculate interparticle potentials can be justified if the volume fraction of clay particles is sufficiently low that most polymer chains interact with no more than two clay sheets at the same time. It can be shown that this requirement is satisfied if the clay volume fraction is not very high ($\Phi < 0.5$) and the radius of gyration of a polymer chain, R_g, is less than the diameter of the clay particle, $R_g < D$. In the system we consider, $N = 300$, $R_g \sim N^{1/2} \approx 17$, so this condition is satisfied.

III. Results and Discussion

To study the influence of the grafted chains on the equilibrium morphology of the mixtures, we consider the following systems: (a) $\rho_{gr} = 0.2$, $N_{gr} = 5$, (b) $\rho_{gr} = 0.04$, $N_{gr} = 25$, (c) $\rho_{gr} = 0.02$, $N_{gr} = 50$, (d) $\rho_{gr} = 0.04$, $N_{gr} = 50$, and (e) $\rho_{gr} = 0.02$, $N_{gr} = 100$. The geometric characteristics of the clay sheets and the length of the polymers in the melt N are kept constant for all the systems: $D = 30$, $L = 1$, $N = 300$. We consider two values of the clay−clay attraction strength, E_0: (1) $E_0 = 0$ (no long-range attraction between clay sheets), and (2) $E_0 = 0.1kT/a^2$ (strong attraction between clay sheets).

The calculation of the phase diagram is performed in two steps. First, we use the SCF model to determine the free energy profiles $U_2(z)$ for each of the five systems, varying the Flory−Huggins parameter χ between +0.05 and −0.05. While this may appear to be a relatively small variation in χ, the SCF results indicate that the system can undergo significant changes in phase behavior (going, for example, from immiscible to intercalated or exfoliated) over this range of values.[14−16] The calculated free energy represents the polymeric contribution to the clay−clay interaction potential. After adding the bare clay−clay interaction potential (described by eq 17), we obtain the potential energy profiles shown in Figures 3a−e and 5a−e. For a fixed z, the polymer−clay interaction is more favorable for lower values of U. Comparison of these profiles allows us to make some qualitative conclusions about the role of grafted chains in determining the equilibrium phase behavior.

We first consider the case $E_0 = 0$. It can be seen, by comparing parts a−c of Figure 3, that for a fixed value of $\theta_t = \rho_{gr}N_{gr}$ (the total amount of grafted monomers), decreasing the grafting density and increasing the length of the grafted chains leads to decreases in the values of $U(z)$. This trend indicates better miscibility between the disks and polymer and, hence, a more repulsive interaction between the disks. The entropy of mixing is greater for polymers and a loose layer of long grafted chains than for polymers and a dense layer of short chains. Furthermore, the longer grafted chains are more effective at providing a steric repulsion between the surfaces. (The steric interaction is due to the entropic elasticity of the grafted chains, which creates an effective repulsion between the surfaces, until the surface separation becomes comparable to the grafted chains' radius of gyration.)

For the range of grafting densities considered here, increasing ρ_{gr} while keeping the chain length constant (see parts c and d of Figure 3) promotes greater mixing between the polymer and clay since the polymers now interact with a "soft" penetrable interface, rather than a hard wall. This observation holds for small grafting densities, where the surfactant molecules are spaced far apart and cannot form monolayers. For such systems, the strength of the effective clay−clay potential increases monotonically with ρ_{gr} (as in parts c and d of Figure 3). At higher grafting densities, the tethered chains form a dense surface layer and the intermixing between the polymers and clay is again unfavorable,[11] as can be seen in Figure 3a, although for a different chain length ($\rho_{gr} = 0.2$, $N_{gr} = 5$). Quantitative determination of the threshold between "favorable" and "unfavorable" grafting densities requires a more systematic study.[61]

Finally, if we keep the grafting density unchanged and vary the length of the grafted chains (see parts b and d of Figure 3 and parts c and e of Figure 3), the strength of the disk−disk repulsion increases as the chain length becomes larger. Thus, from considering all these different cases, one can conclude[14−16] that increasing ρ_{gr} (up to an optimal value) and the length of grafted chains leads to better miscibility between the clay sheets and the polymer melt.

We now turn our attention to the calculation of the (χ, ϕ) phase diagram for each of the five systems. To calculate phase diagrams, we vary the "combined volume fraction" Φ between 0.001 and 0.601 with a step of 0.01. (In Figures 4 and 6, the plots are in units of χ and the "inorganic volume fraction" $\phi = \Phi/(1 + 2\rho_{gr}N_{gr}/L)$.) This procedure is repeated for 13 values of χ in the range −0.05 to +0.05]. (Recall that positive values of χ correspond to the repulsion between the grafted chains and the polymer melt, and, therefore, to effective attraction between the clay disks; negative values of χ correspond to the attraction between the grafted chains and the polymer melt, causing effective repulsion between the clay disks.)

For each point in the (χ, Φ) plane, we calculate free energies of all possible phases. To determine the phase boundaries, we use the Maxwell lever rule for each value of χ. In many cases, the second derivative of the free energy with respect to Φ remains negative even for $\Phi = 0.601$, indicating that the phase separation between the clay and the polymer is "complete" (clay sheets aggregate into large clusters with no polymer inside). In terms of the morphologies in these diagrams, the isotropic or low density nematic phase corresponds to an exfoliated composite. The crystal and columnar phases describe clay-rich crystallites, and the plastic solid phase represents the low-density structure known as a "house of cards" (where clay disks have some positional ordering and prefer "edge-to-face" configurations). The phase diagrams for all five systems are shown in parts a−e of Figure 4.

Let us first comment on the general features of the phase diagrams. In the region where the Flory χ parameter is positive, the systems exhibit a broad phase coexistence between the polymer-rich isotropic phase and the clay-rich crystal phase. Such behavior corresponds to a strong immiscibility between the organically modified clay and the polymer matrix; clay sheets, even if exfoliated during processing, will eventually reaggregate. As $\chi \to 0$, the two-phase region becomes narrower and splits into two (isotropic−nematic and nematic−crystal). The triple point (I−N−Cr) is dependent on the specific system parameters, as is the width of the nematic phase. For the systems under consideration, the smectic phase was always found to be metastable (within the broad isotropic−crystal coexistence). When χ becomes negative, the isotropic−nematic and nematic−crystal coexistence regions become narrower and shift toward higher values of ϕ. Finally, when χ is strongly negative, the new "plastic solid"[62] ("house-of-cards"[31]) and columnar phases appear. Indeed, at low clay loadings, the strong repulsion between neighboring disks forces them to adopt more energetically favorable "edge-to-face" configurations. This leads to either gelation or crystallization. At higher clay volume fractions, the steric excluded volume effects dominate the long-range disk−disk repulsion, forcing the formation of columnar and crystal phases.

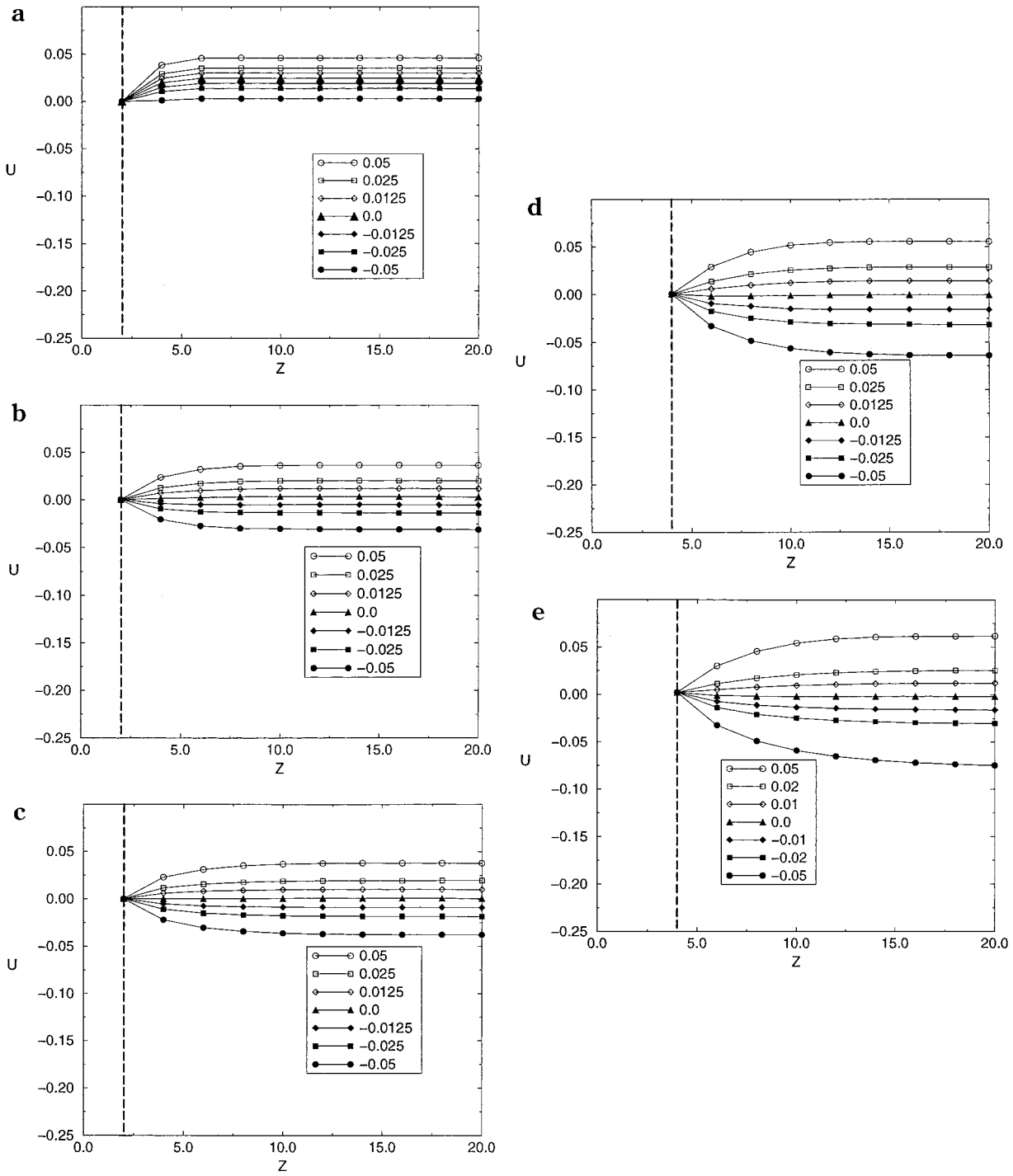

Figure 3. Free energy of interaction, U, as a function of separation, Z, for two parallel plates with grafted chains: (a) $\rho_{gr} = 0.2$, $N_{gr} = 5$, (b) $\rho_{gr} = 0.04$, $N_{gr} = 25$, (c) $\rho_{gr} = 0.02$, $N_{gr} = 50$, (d) $\rho_{gr} = 0.04$, $N_{gr} = 50$, and (e) $\rho_{gr} = 0.02$, $N_{gr} = 100$. The dashed vertical lines on each plot denote the "hard-wall" condition (Z cannot be smaller than $2\rho_{gr}N_{gr}$ because of the incompressibility of the polymer melt and the grafted chains). The attractive strength $E_0 = 0$.

We now analyze the dependence of the phase behavior on the surfactant length and the grafting density. It can be easily seen that the phase diagrams plotted in parts d ($\rho_{gr} = 0.04$, $N_{gr} = 50$) and e ($\rho_{gr} = 0.02$, $N_{gr} = 100$) of Figure 4 are very similar. The phase diagrams shown in parts b ($\rho_{gr} = 0.04$, $N_{gr} = 25$) and c ($\rho_{gr} = 0.02$, $N_{gr} = 50$) of Figure 4 are also very similar to each other. One can conclude, therefore, that the macroscopic phase behavior of the polymer−clay mixture is primarily determined by the total amount of surfactant θ_t. This statement holds for relatively long surfactants and relatively low grafting densities. For the case of short densely grafted organic modifiers (Figure 4a), the immiscibility between the clay disks and polymer (see Figure 3a) dominates the phase behavior of the system.

To study the dependence of the phase behavior of the mixture on the surfactant length, N_{gr}, we compare the diagrams plotted in parts b ($\rho_{gr} = 0.04$, $N_{gr} = 25$) and d ($\rho_{gr} = 0.04$, $N_{gr} = 50$) of Figure 4. It can be seen that increasing N_{gr} moves the isotropic−nematic−crystal triple point upward (from $\chi \approx 0.02$ in Figure 4b to $\chi \approx 0.05$ in Figure 4d) and extends the stability region of the nematic phase to more positive values of χ. It also

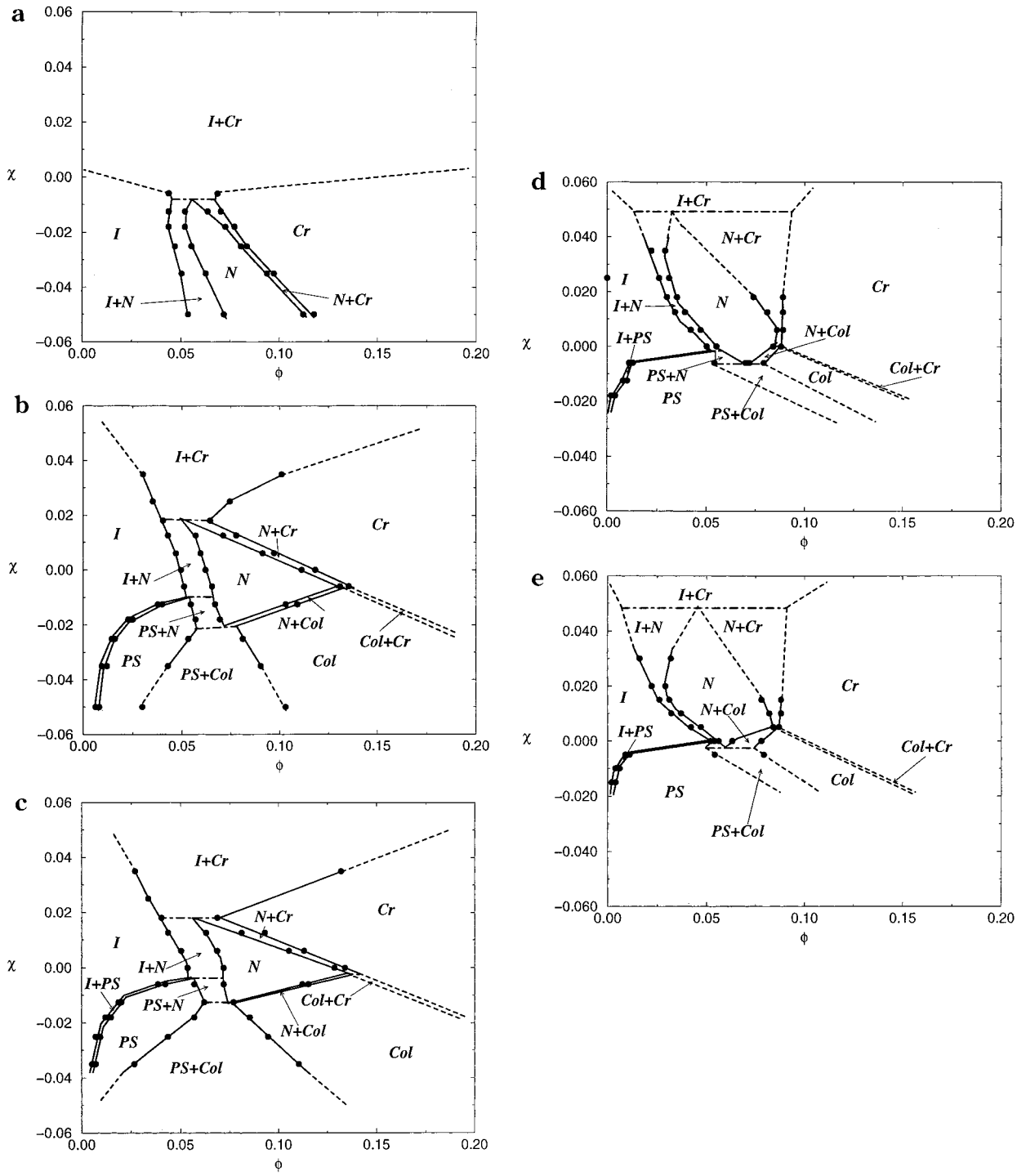

Figure 4. Phase diagrams of polymer−clay mixtures: (a) $\rho_{gr} = 0.2$, $N_{gr} = 5$, (b) $\rho_{gr} = 0.04$, $N_{gr} = 25$, (c) $\rho_{gr} = 0.02$, $N_{gr} = 50$, (d) $\rho_{gr} = 0.04$, $N_{gr} = 50$, and (e) $\rho_{gr} = 0.02$, $N_{gr} = 100$. Phases: I, isotropic; N, nematic; Cr, crystal; PS, plastic solid; Col, columnar. Points represent calculated coexistence densities; lines serve as guide to the eye. Dashed lines represent approximate locations of phase transition boundaries (exact calculation was impossible because one or both coexistence points lie in the region $\Phi > 0.6$). ϕ is the clay volume fraction, and χ is the Flory−Huggins χ-parameter between the surfactant and the polymer.

narrows the two-phase isotropic−nematic region. All these effects are favorable in creating thermodynamically stable exfoliated composites. The only adverse factor from increasing N_{gr} is the narrowing of the nematic phase near $\chi = 0$. Indeed, with the increase in the total amount of surfactant, we simultaneously increase the effective excluded volume of the clay particles and decrease the shape anisotropy (see eq 9). As a result, the maximum "inorganic volume fraction" where one can obtain an orientationally ordered exfoliated morphology is decreased dramatically (from $\phi = 0.12$ in Figure 4b to $\phi = 0.07$ in Figure 4d). Similar conclusions can be drawn by comparing parts c ($\rho_{gr} = 0.02$, $N_{gr} = 50$) and e ($\rho_{gr} = 0.02$, $N_{gr} = 100$) of Figure 4.

Finally, we consider the case where one changes the grafting density ρ_{gr} while keeping N_{gr} constant. It is easy to conclude, by comparing parts c ($\rho_{gr} = 0.02$, $N_{gr} = 50$) and d ($\rho_{gr} = 0.04$, $N_{gr} = 50$) of Figure 4, that the effect of increasing ρ_{gr} (within the narrow range considered here) improves the miscibility and enhances the ther-

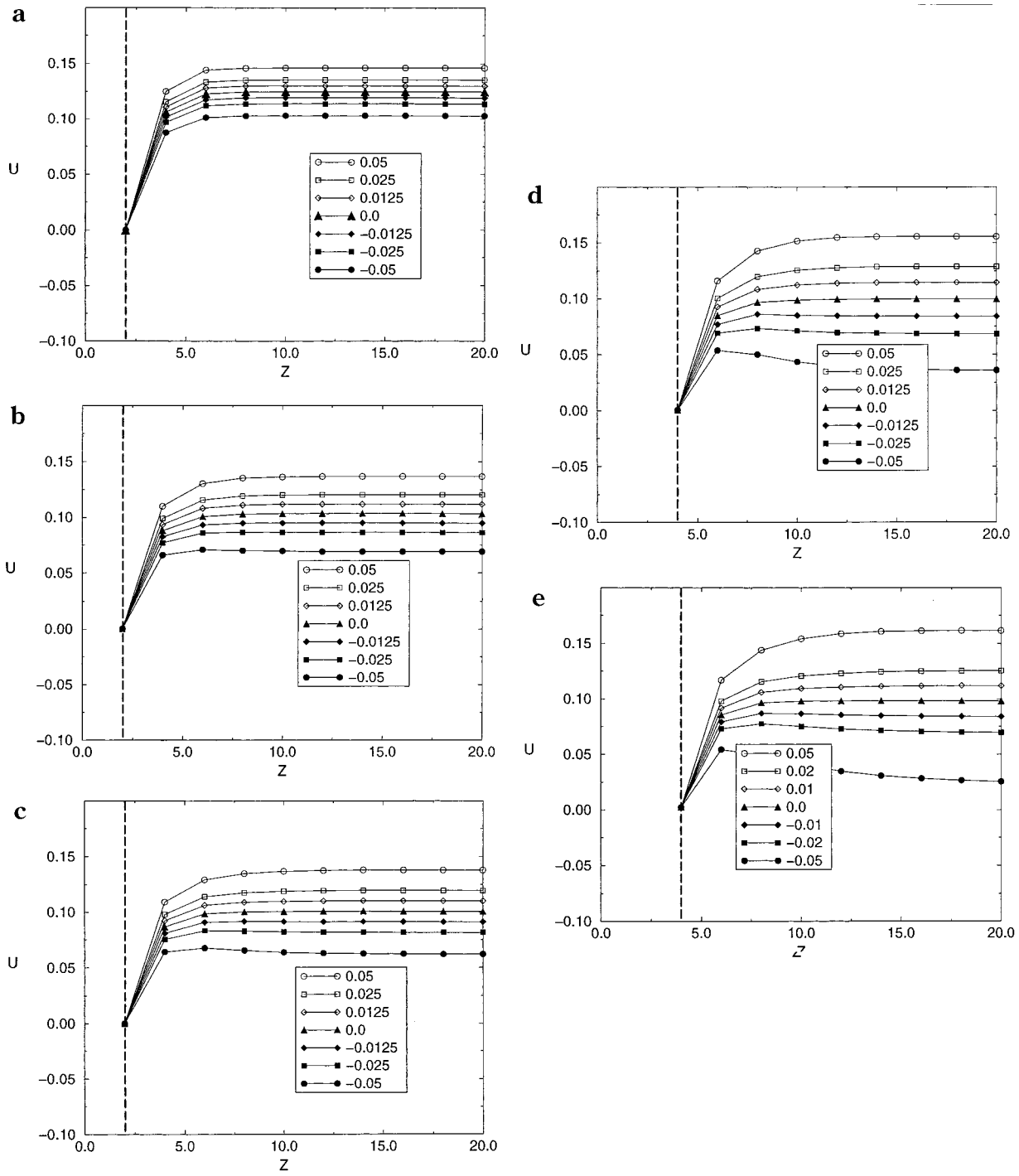

Figure 5. Same as Figure 3, but with $E_0 = 0.1$.

modynamic stability of the dispersed composite morphologies (isotropic and nematic phases).

In the above analysis, we assume that the clay particles have only excluded-volume interactions ($E_0 = 0$). In many real systems, there is a strong van der Waals interaction between the clay sheets that inhibits exfoliation. To model this effect and its influence on the phase behavior, we repeated all the calculations with $E_0 = 0.1$, mimicking a strong clay−clay attraction. The effective potentials (consisting of both a clay−clay attraction term U_1 and a polymer-mediated interaction U_2) are plotted in parts a−e of Figure 5. We now calculate the phase diagrams and see how the addition of the clay−clay attraction modifies the phase behavior.

For the systems with $\theta_t = 1$, the clay−clay attraction completely dominates the entropic contribution of the surfactant molecules. The phase diagrams (not plotted here) show the complete immiscibility between polymer and clay for all values of χ in the −0.05 to +0.05 range. For the systems with $\theta_t = 2$ (parts a and b of Figure 6), the miscibility is significantly diminished relative to the corresponding $E_0 = 0$ cases (see parts d and e of Figure 4), as one would expect. The isotropic−nematic-crystal triple point is shifted downward from $\chi \approx 0.05$ ($E_0 = 0$, Figure 4d) to $\chi \approx 0.02$ ($E_0 = 0.1$, Figure 6a). The total areas occupied by isotropic and nematic phases shrink dramatically, and the nematic−crystal transition occurs at lower values of ϕ.

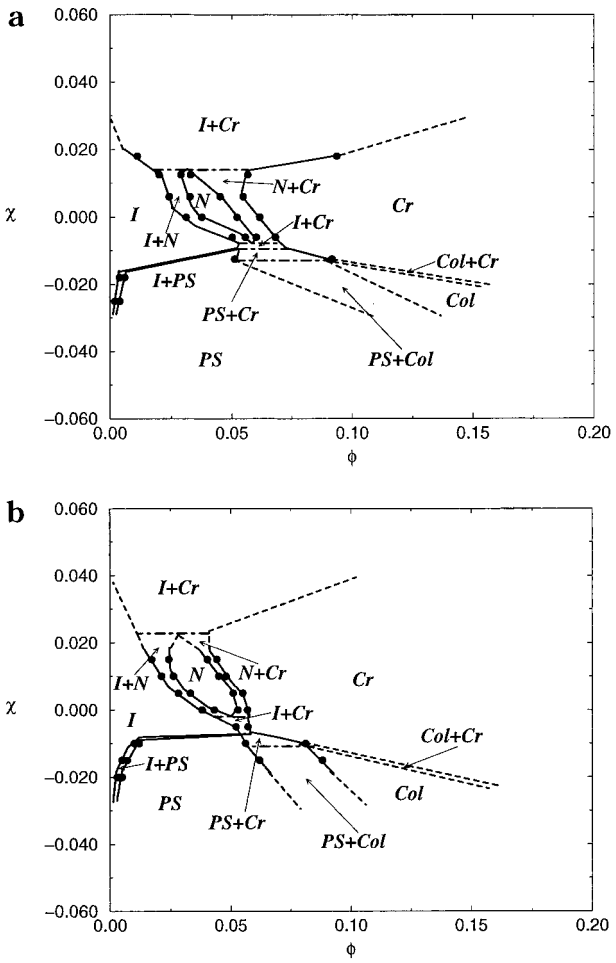

Figure 6. Phase diagrams of polymer−clay mixtures: (a) $\rho_{gr} = 0.04$, $N_{gr} = 50$, and (b) $\rho_{gr} = 0.02$, $N_{gr} = 100$. $E_0 = 0.1$. The phase diagrams for the other three systems are not shown because for all $-0.05 < \chi < +0.05$ polymer and clay are completely immiscible.

The calculated phase diagrams suggest qualitative trends in the macroscopic phase behavior of polymer−clay nanocomposites. At the same time, quantitative comparison of phase diagrams of model and currently studied experimental systems is somewhat difficult. Typically, the surfactant molecules range in length between 10 and 20 CH_2 groups, and the grafting density is quite high (1−3 chains/nm^2).[11] More systematic experimental studies involving longer grafted chains are needed to test our predictions.

It is important to note that the calculated phase diagrams describe only the equilibrium properties of the polymer−clay mixtures. As suggested in ref 34, to understand the exfoliation process in polymer−clay nanocomposites, one has to consider the kinetic aspects of the penetration of polymer into the gap between the clay sheets. The analysis of kinetic factors is beyond the scope of this study. However, assuming that the separation of clay particles has occurred, the phase diagrams calculated here describe the equilibrium morphology of the resulting composite.

IV. Conclusions

We developed a thermodynamic, multiscale approach to study the phase behavior of model polymer−clay mixtures. To describe the ordering of the clay particles, we used the Somoza−Tarazona free energy functional and considered isotropic, nematic, smectic, columnar, crystal, and plastic solid phases. The long-range interaction between the clay sheets is calculated using the self-consistent field approximation. This approach allows us to explicitly take into account the characteristics of grafted organic modifiers and the strength of their interactions with the polymer melt or solution.

One motivation for these studies arose from the findings of the previous SCF calculations.[14−16] In particular, the prior results revealed that significantly increasing the length of the surfactants (beyond the typically used C_{12}−C_{20}) to polymeric-like values can enhance the thermodynamic stability of exfoliated hybrids. In this paper, we used the combined DFT−SCF method to determine how these tendencies translate into the macroscopic phase behavior of the mixtures.

The calculated phase diagrams are in qualitative agreement with the predictions that emerged from an investigation of the SCF-generated free energy profiles. As the length of the grafted chains and/or their density is increased, the miscibility between the clay sheets and the polymer is improved, and the resulting mixture can exhibit an exfoliated (isotropic or nematic) structure for a range of clay volume fractions. For small values of N_{gr} (short surfactant molecules), the polymer is unable to penetrate the gallery between the clay surfaces, and the equilibrium morphology becomes immiscible (two-phase) for most values of the Flory−Huggins parameter and the clay volume fraction. Only in the limit of large negative χ (strong attraction between grafted chains and polymer melt) can such a composite become exfoliated.

The calculated phase diagrams show that the phase stability of polymer−clay nanocomposites is extremely sensitive to the specific features of clay−clay, clay−polymer, and surfactant−polymer interactions. To achieve an accurate quantitative description of the phase behavior in these systems, one has to correctly describe all these interactions using realistic molecular simulation techniques (see, for example, ref 60), which is beyond the scope of the current study. At the same time, the general structure of the phase diagrams, especially the phase behavior at small positive χ, where the polymer-rich isotropic phase coexists with a highly ordered clay-rich phase, agrees well with some recent experimental observations.[12,63,64]

The proposed method can be easily applied to other polymer−colloid systems where the anisotropy of colloidal particles plays an important role. The findings can be used in the design of new polymer-inorganic composites.

Acknowledgment. This work was supported by the Dow Chemical Co., the Army Office of Research, the NSF through Grant No. DMR-9709101 and ONR through Grant N00014-91-J-1363. Part of the calculations in this study were carried out on the computers in the Laboratory of Molecular and Materials Simulations, University of Pittsburgh, funded by the NSF and by a grant from IBM Corp. We thank Drs. David Moll, Ekaterina Zhulina, Dmitri Kuznetsov, and June Huh for useful discussions.

Appendix A: Smoothed Density Approximation

The smoothed density functional $\bar{\Phi}(\mathbf{r})$ is given by

$$\bar{\Phi}(\mathbf{r}) = v_c\bar{\rho}(\mathbf{r}) = v_c \int d\mathbf{R}\, \rho(\mathbf{r})w(|\mathbf{r} - \mathbf{R}|,\bar{\rho}) \quad \text{(A1)}$$

where the effective volume $v_c = V_c(1 + 2\rho_{gr}N_{gr}/L)$, and

the normalized weight function $w(|\mathbf{r} - \mathbf{R}|, \bar{\rho})$ is used to smooth (coarse-grain) density variations. For ellipsoids, it is given by

$$w(|\mathbf{r}|, \bar{\rho}) = w_0(|\mathbf{s}|) + \bar{\rho} w_1(|\mathbf{s}|) + \bar{\rho}^2 w_2(|\mathbf{s}|) \quad \text{(A2)}$$

where $\mathbf{s}$ is the normalized distance defined by $\mathbf{r} = \sum \mathbf{s}$ ($\sum$ is a diagonal matrix whose elements are three lengths of the ellipsoid σ_x, σ_y, σ_z). Functions $w_0(s)$, $w_1(s)$, and $w_2(s)$ are derived in ref 40. Equations Al−A2 are nonlinear and must be solved numerically to determine smoothed profile $\bar{\rho}(\mathbf{r})$ for any given single-particle density $\rho(\mathbf{r})$.

References and Notes

(1) Giannelis, E. P.; Krishamoorti, R.; Manias, E. *Adv. Polym. Sci.* **1999**, *138*, 107 and references therein.
(2) Okada, A.; Kawasumi, M.; Kojima, Y.; Kuraichi, T.; Kamigaito, O. *Mater. Res. Soc. Symp. Proc.* **1990**, *171*, 45.
(3) Yano, K.; Uzuki, A.; Okada, A.; Kuraichi, T.; Kamigaito, O. *J. Polym. Sci., Part A: Polym. Chem.* **1993**, *31*, 2493.
(4) Kojima, Y.; Uzuki, A.; Kawasumi, M.; Okada, A.; Kuraichi, T.; Kamigaito, O. *J. Polym. Sci., Part A: Polym. Chem.* **1993**, *31*, 983.
(5) Uzuki, A.; Kawasumi, M.; Kojima, Y.; Okada, A.; Kuraichi, T.; Kamigaito, O. *J. Mater. Res.* **1993**, *8*, 1174.
(6) Vaia, R. A.; Jandt, K. D.; Kramer, E. J.; Giannelis, E. P. *Macromolecules* **1995**, *28*, 8080.
(7) Lan, T.; Kaviratna, P. D.; Pinnavaia, T. J. *Chem. Mater.* **1995**, *7*, 2144.
(8) Vaia, R. A.; Sauer, B. B.; Tse, O. K.; Giannelis, E. P. *J. Polym. Sci., Part B: Polym. Phys.* **1997**, *35*, 59.
(9) Messersmith, P: B.; Stupp, S. I. *J. Mater. Res.* **1992**, *7*, 2599.
(10) Krishnamoorti, R.; Vaia, R. A.; Giannelis, E. P. *Chem. Mater.* **1996**, *8*, 1728.
(11) Vaia, R. A.; Giannelis, E. P. *Macromolecules* **1997**, *30*, 7990, 8000.
(12) Vaia, R. A.; Jandt, K. D.; Kramer, E. J.; Giannelis, E. P. *Chem. Mater.* **1996**, *8*, 2628.
(13) Muzny, C. D.; Butler, B. D.; Hanley, H. J. M.; Tsvetkov, F.; Peiffer, D. G. *Mater. Lett.* **1996**, *28*, 379.
(14) Balazs, A. C.; Singh, C.; Zhulina, E. *Macromolecules* **1998**, *31*, 8370.
(15) Zhulina, E.; Singh, C.; Balazs, A. C. *Langmuir* **1999**, *15*, 3935.
(16) Balazs, A. C.; Singh, C.; Zhulina, E.; Lyatskaya, Y. *Accounts of Chem. Research* **1999**, *32*, 651.
(17) Balazs, A. C.; Singh, C.; Zhulina, E. Designing Exfoliated Polymer/Clay Composites Through Self-consistent Field Theory. In *Microstructure and Tribology of Polymer Surfaces*; Wahl, K. J., Tsukruk, V., Eds.; Plenum Press: in press.
(18) Asakura, S.; Oosawa, F. *J. Chem. Phys.* **1954**, *22*, 1255.
(19) Vrij, A. *Pure Appl. Chem.* **1976**, *48*, 471.
(20) Gast, A. P.; Hall, C. K.; Russel, W. B. *J. Colloid Interface Sci.* **1983**, *96*, 251.
(21) Poon, W. C. K.; Selfe, J. S.; Robertson, M. B.; Illett, S. M.; Pirie, A. D.; Pusey, P. N. *J. Phys. II Fr.* **1993**, *3*, 1075.
(22) Meijer, E. J.; Frenkel, D. *Phys. Rev. Lett.* **1991**, *67*, 1110.
(23) Lekkerkerker, H. N. W.; Poon, W. C. K.; Pusey, P. N.; Stroobants, A.; Warren, P. B. *Europhys. Lett.* **1992**, *20*, 559.
(24) Meijer, E. J.; Frenkel, D. *J. Chem. Phys.* **1994**, *100*, 6873.
(25) Illett, S. M.; Orrock, A.; Poon, W. C. K.; Pusey, P. N. *Phys. Rev. E* **1995**, *51*, 1344.
(26) Dijkstra, M.; van Roij, R.; Evans, R. *Phys. Rev. Lett.* **1999**, *82*, 117.
(27) Gast, A. P.; Russel, W. B. *Physics Today* **1998**, *12*, 24 and references therein.
(28) Bolhuis, P. G.; Stroobants, A.; Frenkel, D.; Lekkerkerker, H. N. W. *J. Chem. Phys.* **1997**, *107*, 1551.
(29) Adams, M.; Dogic, Z.; Keller, S. L.; Fraden, S. *Nature* **1998**, *393*, 349 and references therein.
(30) Dijkstra, M.; van Roij, R. *Phys. Rev.* E **1997**, *56*, 5594.
(31) Dijkstra, M.; Hansen, J. P.; Madden, P. A. *Phys. Rev. E* **1997**, *55*, 3044.
(32) Bates, M.; Luckhurst, G. R. *J. Chem. Phys.* **1996**, *104*, 6696.
(33) Gay, J. G.; Berne, B. J. *J. Chem. Phys.* **1981**, *74*, 3316.
(34) Lyatskaya, Y.; Balazs, A. C. *Macromolecules* **1998**, *31*, 6676.
(35) Ginzburg, V. V.; Balazs, A. C. *Macromolecules* **1999**, *32*, 5681.
(36) Onsager, L. *Ann. N.Y. Acad. Sci.* **1949**, *51*, 627.
(37) Liu, A. J.; Fredrickson, G. *Macromolecules* **1993**, *26*, 2817.
(38) Brochard, F.; Jouffroy, J.; Levinson, P. *J. Phys. (Fr.)* **1984**, *45*, 1125.
(39) Chiu, H.-W.; Kyu, T. *J. Chem. Phys.* **1995**, *103*, 7471; *Phys. Rev. E* **1996**, *53*, 3618; *J. Chem. Phys.* **1997**, *107*, 6859.
(40) Tarazona, P. *Phys. Rev. A* **1985**, *31*, 2673.
(41) Somoza, A. M.; Tarazona, P. *J. Chem. Phys.* **1989**, *91*, 517.
(42) We note that it is possible to introduce a polymer-surface χ, as well as a surfactant-surface χ, into the SCF calculation.[16] We can then calculate phase diagrams using these potentials and determine the influence of such interactions on the macroscopic phase behavior. This will be the subject of future studies.
(43) Flory, P. J. *Principles of Polymer Chemistry*; Cornell University Press: Ithaca, NY, 1953.
(44) Schaink, H. M.; Smit, J. A. M. *Macromolecules* **1996**, *29*, 1711.
(45) Kventsel, G. F.; Luckhurst, G. R.; Zewdie, H. B. *Mol. Phys.* **1985**, *56*, 589.
(46) Scheutjens, J. M. H. M.; Fleer, G. J. *J. Phys. Chem.* **1979**, *83*, 1619.
(47) Fleer, G.; Cohen-Stuart, M. A.; Scheutjens, J. M. H. M.; Cosgrove, T.; Vincent, B. *Polymers at Interfaces*; Chapman and Hall: London, 1993; Chapter 5.
(48) Fleer, G. J.; Scheutjens, J. M. H. M. *J. Colloid Interface Sci.* **1986**, *111*, 504.
(49) Zhulina, E. B.; Halperin, A. *Macromolecules* **1992**, *25*, 5730 and references therein.
(50) Schweizer, K. S.; Yetiraj, A. *J. Chem. Phys.* **1993**, *98*, 9080.
(51) Chatterjee, A. P.; Schweizer, K. S. *Macromolecules* **1999**, *32*, 923 and references therein.
(52) Szleifer, I.; Ben-Shaul, A.; Gelbart, W. M. *J. Phys. Chem.* **1990**, *94*, 5081.
(53) Ramakrishnan, T. V.; Yussouf, M. *Phys. Rev. B* **1979**, *19*, 2775.
(54) Velasco, E.; Somoza, A. M.; Mederos, L. *J. Chem. Phys.* **1995**, *102*, 8107.
(55) Ginzburg, V. V.; Glaser, M. A.; Clark, N. A. *Liq. Cryst.* **1997**, *23*, 227.
(56) Carnahan, N. F.; Starling, K. E. *J. Chem. Phys.* **1969**, *51*, 635.
(57) Vroege, G. J.; Lekkerkerker, H. N. W. *Rep. Prog. Phys.* **1992**, *55*, 1241.
(58) Luckhurst; G. R.; Simmonds, P. S. J. *Mol. Phys.* **1993**, *80*, 233.
(59) Sokolova, E. P.; Vlasov, A. Yu. *Liq. Cryst.* **1990**, *8*, 47.
(60) Hackett, E.; Manias, E.; Giannelis, E. P. *J. Chem. Phys.* **1998**, *108*, 7410.
(61) While it would be useful to determine the optimal value of ρ_{gr} for each value of N_{gr}, such a calculation is beyond the scope of this paper. It can be done by varying ρ_{gr} for a fixed N_{gr}, calculating and then comparing the SCF free energy curves. For more detailed discussion, see ref 16.
(62) Frenkel, D. *Mol. Phys.* **1987**, *60*, 1.
(63) Vaia, R. A. Private communication.
(64) Russel, T. P. Private communication.

MA991324E